OPTIMIZATION OF MAGNETICALLY ACTUATED STEEL SCANNNER SYSTEMS

by
Gökçe AKÖZ

Submitted to the Institute of Graduate Studies in
Science and Engineering in partial fulfillment of
the requirements for the degree of
Master of Science
in
Electrical and Electronics Engineering

Bilgi University
2018

OPTIMIZATION OF MAGNETICALLY ACTUATED
STEEL SCANNNER SYSTEMS

Gökçe AKÖZ
116815003

Tez Danışmanı: Dr. Öğr. Üyesi Yiğit Dağhan GÖKDEL ……....
İstanbul Bilgi Üniversitesi
Mühendislik ve Doğa Bilimleri Fakültesi

Jüri Üyeleri: Dr. Öğr. Üyesi Baykal SARIOĞLU ……..…
İstanbul Bilgi Üniversitesi
Mühendislik ve Doğa Bilimleri Fakültesi

Dr. Öğr. Üyesi Ceyhun KIRIMLI ……...
Acıbadem Mehmet Ali Aydınlar Üniversitesi
Mühendislik Fakültesi

Tezin Onaylandığı Tarih: ……
Toplam Sayfa Sayısı: …….

Anahtar Kelimeler (Türkçe)	Anahtar Kelimeler (İngilizce)
1) Mikro Elektro Mekanik Sistemler	1) Microelectromechanical Systems
2) Tarayıcı	2) Scanner
3) Manyetik hareket ettirme	3) Magnetic actuation
4) Elektro bobin	4) Electro-coil
5) Denk manyetik devre	5) Equivalent magnetic circuit

ACKNOWLEDGEMENTS

First of all, I express my sincere gratitude to Y. Dağhan GÖKDEL, my supervisor. I'm excessively indeeded to him for his precious guidance and encouragement offered to me.

Then, I would like to present separately thanks of my gratitude to each of my family members for their valuable support and implacable encouragement as well.

I take also opportunity to submit my sincere appreciations to my dear team members, Ayşin ARSEVEN and Ahmet AY, with whom I have worked in Microsystems Laboratory and who provided technical and moral full support.

Finally, I would like to present all my gratitude to one and all and also my lovely friends, who directly and or indirectly shared these two years of thesis with me and motivated me.

ABSTRACT

OPTIMIZATION OF MAGNETICALLY ACTUATED STEEL SCANNNER SYSTEMS

This thesis presents optimization of a novel two dimensional magnetically actuated scanner design. Various scanners are conceived and simulated. Then the best new scanner design is chosen. Purposed scanner dimensions are 16 mm x 16 mm and 570 μm thickness. This scanner offers two dimensional orthogonal scanning features.

Within the context of magnetic actuation of scanner is provided by and electro-coil. This electro-coil parameters are expressed analytically and then an electro-coil is designed in accordance with these parameters in order to ensure magnetic actuation of stainless steel scanner. Finally, magnetic actuation is provided by an electro-coil of 4 mm radius, 8 mm of diameter and 12 mm length.

Consequently, for more appropriate position for electro-coil in x, y and z directions and angle with respect to scanner are optimized for having a relatively high total optical scan angle.

ÖZET

MANYETİK HAREKET ETTİRİLEN ÇELİK TARAYICI SİSTEMLERİN OPTİMİZASYONU

Bu tez, 2 boyutlu dik tarama yapan, manyetik hareket ettirilen yeni tasarlanan tarayıcının optimizasyonunu sunmaktadır. Birçok tarayıcının tasarımı ve benzetimi yapılmıştır. İstenilen özelliklere en uygun, 16 mm x 16 mm boyutunda, 570 µm kalınlığındaki, iki boyutlu tarama yapabilen tarayıcı seçilmiştir. Manyetik hareketini sağlamak amacıyla bobin kullanımı tercih edilmiştir. Bu bobin tanımlanan parametreler kullanılarak manyetik alan formülü elde edilmiştir. Bu parametrelere uygun olarak çelik mikro tarayıcının en iyi şekilde manyetik hareketini sağlamak amacıyla tasarlanmıştır. Manyetik hareketi sağlayan bobin, 4 mm yarıçapında ve 12 mm uzunluğundadır.

Sonuç olarak, olabilecek en yüksek optik tarama açısını elde edebilmek amacıyla, tarayıcı ve bobinin x, y ve z eksenlerinde ve θ açısına en uygun konumu bulunmuştur.

TABLE OF CONTENTS

LIST OF FIGURES

LIST OF TABLES

LIST OF ABBREVIATION / SYMBOLS

MEMS	Micro Electro Mechanical Systems
TOSA	Total Optical Scan Angle
SS	Stainless Steel
DMD	Digital- Mirror-Devices (Texas Instruments)
LIDAR	Light Detection and Ranging
MMF	Magnetomotive Force
FEM	Finite Element Modeling
LDV	Laser Doppler Vibrometer

1. INTRODUCTION

Miniaturization with a high working performance and low power consumption renders Micro Electro Mechanical Systems (MEMS) structures more interesting for various applications.

Optical applications of MEMS came up in the form such as projection displays based on micromachined two-dimensional spatial-light modulators in 1970s. Earlier devices are developed and commercialized by Texas Instruments Digital- Mirror-Devices (DMD) [1]. In this optical domain, the first scanning silicon mirror in literature was published in 1980 [2].

Briefly, optical MEMS scanners can be classified according to (1) their *operation principle* (reflective mirror, refractive lens etc), (2) their *actuation principle* (magnetic [3-5], electrostatic [6], piezoelectric [7], thermal [8], etc) and their (3) *fabrication technology* [2].

One of the most frequently used microstructures in optical MEMS can be stated as MEMS scanners. These MEMS scanners are employed as an imaging device in laser scanning confocal microscopy, endoscopy applications, bar code scanning, medical imaging, LIDAR systems and communication systems where scanning angles are particularly important. For instance, bar code scanner requires a large scanning angle at low frequency values [1][9-10].

Constitutively, MEMS scanners requirements to improve scanning performance are scan angle, mirror size, mirror flatness and mode separation for resonant scanners. Moreover, resonant scanners require a high quality factor value in order to increase scan angles [2]. For non-resonant scanners linearity can be stated as the basic parameter [11]. It is also important to take trade off between scan angle and mirror width in consideration. This trade off with respect to resolution is discussed in details in [12].

Various scanner designs having total optical scan angles (TOSA) varying from 7° to 105° are reported in literature. As the best example, electrostatically actuated polysilicon micro-scanner that has achieved to 86° of TOSA at its resonance frequency, 30.8 kHz can be given [12]. Magnetically actuated two-dimensional (2D) scanner can scan 53° and 65° at 21.3 kHz (fast scan) and 60 Hz (slow scan), respectively [4]. A magnetically actuated steel scanner has achieved 105° as TOSA [13]. Scanning angles of different micro- scanners are reported and are compared in [11]. Various total optical scan angles achieved in literature is given in Table 1.1.

Table 1.1. Various total optical scan angles in literature

Total Optical Scan Angle (TOSA)	**Reference**	**Total Optical Scan Angle (TOSA)**	**Reference**
20°	[1]	65° (slow scan) and 53° (fast scan)	[4]
7.6°	[14]	16°	[15]
-20.3°(slow scan) and 15.6°(fast scan)	[16]	76° (slow scan) and 5.9° (fast scan)	[13]
16°	[3]	105° (slow and fast scan)	[13]
86°	[17]	88°	[5]

Concerning actuation schemes of micro structures, because of speed and ease of actuation and control mainly there are two common methods: electrostatic and magnetic actuation. Among of several actuation schemes, magnetic actuation is preferred since it provides larger displacements by consuming low power (Ataman, Lani, Noell, & Rooji, 2012) [13][18-19][20-23]. It enables also simple microfabrication and electrical contacts are avoided. Therefore, magnetic actuation scheme is commonly used for MEMS scanning applications. Magnetic actuation can be evaluated regarding the following principles: fabrication, displacement, power consumption and linearity.

Holmström et al. compares properties of different actuation principles in Table 1.2. This table is given below:

Table 1.2. Comparison of Actuation Methods [2]

Category	**Electrostatic**	**Magnetic**	**Piezoelectric**
Preferred Type	Comb drive	Moving coil	PZT film
Simple Fabrication	+ + +	+ + +	+ +
Large Displacement	+ +	+ + +	+
High Force	+	+ +	+ + +
Low Power	+ +	+	+ + +
Low Voltage	+	+ + +	+ +
Compactness	+ + +	+	+ + +
Linearity	+	+ + +	+ +

Once magnetic actuation is preferred, it can be performed by two main schemes: moving magnet and moving coil schemes. External magnets can also be used in order to generate a static magnetic field. Thereby, the moving element is an electro-coil which has little mass. In order to utilize magnetic field in an efficient way, position of coil or magnet and magnetic material properties are taken in account. Meanwhile, coils angular position according to micro-system is significant not only to make use of maximum magnetic field but also to trigger simultaneously fast scan and slow scan frequencies. For this reason, coils are positioned with an inclination as 45° [4][23-24].

Materials relative magnetic permeability value plays a considerable role to obtain large deflections without the need for strong magnetic fields and therefore strong currents. Among magnetic materials, for instance, stainless (structural) steel (SS) represents higher relative magnetic permeability as a fabrication material [24] and also they have better mechanical behaviour than iron.

Furthermore, scanner design provides a 2D scanning where one of the scanning modes corresponds to torsional mode [22][25-26]. A scanner fabricated out of steel can reach to higher resonant frequencies compared to other scanners structured with other materials. Steel mechanical scanners demonstrate better performance levels for horizontal and vertical resolution and also scan-angle point of view [21]. Ease of getting the material and its low-cost as well as longevity makes SS preferable.

In conclusion, many scanners are designed in order to provide maximum TOSA for distinct applications. Fundamentally, proposed designs aimed to improve optical scanning properties and features as well.

This thesis aims to optimize total optical scanning angle of a magnetically actuated of a proposed stainless steel grade 430 scanner. Magnetic power of the actuation system is provided by a custom electro-coil. Position for electro-coil with respect to scanner is optimized in x, y and z directions and α, angle between scanner and electro-coil to improve the total delivered magnetic power with minimal electrical power consumed and hereby the total optical scan angle of the system.

2. PROPOSED DESIGN

In this section, a new stainless steel micro- scanner design is discussed to successfully deliver a raster scanning.

Orthogonal scanning is desired in order to provide scanning in two dimensions: horizontal and vertical. Thus, by this scanning method two dimensional imaging can be realized.

This new scanner design targets to suit some restrictions on frequency, size, weight, power, displacement, resolution. Miniaturizing systems necessitates effectively reducing display size by increasing frequency values and decreasing power consumption [11-12]. Design parameters to enhance scanning features can be listed as follows: displacement, quality factor, geometry, physical conditions of laboratory. Resolution, frequency, scanner deformation, stress, cost are determined by design variables. All design parameters are interrelated. Highest resolution is achieved by an optimal choice of all parameters. [12] proposes a table concerning scanner performance associated to design parameters. θ is maximum scan angle, D is mirror width, t is thickness of mirror, a and b are half width of flexure and half thickness of flexure, respectively, L_f is flexure length and λ is wavelength of light.

Table 2.1. Scanner performance to associated design parameters

Design Parameter	**θ**	**D**	**t**	**a, b**	**L_f**	**λ**	**Material**
Resolution	x	x				x	
Frequency		x	x	x	x		x
Mirror deformation upper limit	x	x	x			x	x
Flexure stress upper limit	x			x	x		x
Optical and mechanical design limits	x	x				x	
Cost and package size		x			x		x

Fast and slow scanning frequencies correspond to two distinct modes of raster scanning frequencies. High proportion between these two frequency values leads a raster scan with a better resolution. In the other words, to achieve a good scan, two modes must be separated. Substantially, separation of two modes ensures high mechanical quality (Q) factor [15].

In order to obtain high quality factor and to minimize power consumption, it is essential to have separated scanning frequency values from torsional mode frequency and its harmonics. When mode frequency ratio increases, quality factor proportionally increases. Moreover, at resonance frequencies, while scanner is running at resonant frequency, least amount of power is required [21]. Since the displacement is increased by the quality factor value, to have mode frequency ratio as large as possible, torsional mode frequency should be the first mode. In the other words, torsional mode frequency must correspond to the smallest frequency where the other mode frequency has a value considerably far from torsional mode frequency [15][21-22][24].

Scanning frequency values depend particularly on geometry. It is determined by 3D shape of scanner and properties of the structural material. More specifically, resonance frequency is related to mirror and flexure dimensions. For large scan angle at high frequency, little inertia and high stiffness are required. While determining resonance frequency, it is necessary to adjust mirror size and mirror thickness. As a rule of thumb, one can state that small scanner dimensions increase resonance frequency. In other words, resonance frequency is both inversely proportional to mirror size (Urey, Wine, & Lewis, Scanner Design and Resolution Tradeoffs for Miniature Scanning Displays, 1999) and to substantial decrease of flexure length [24].

Furthermore, it is also important to note that, increasing mirror dimensions also increases the mass of scanner and it also slows the scanning frequency as well [12] [24]. Since inertia of micro scanner plays a role on scanning frequency values, mass of mirror must be increased to augment inertia. Therefore, solid part on low scan frequency scanning axe should be increased and filled.

Determination of geometry brings stress and strain notions as well. These two notions depend principally on material properties. Under same conditions, [27-28] indicates that a

circular plate reveals the most deflection because of distribution of inertia moment for same mass compared to rectangular and square shapes. In literature, there are scanner designs possess circular shape mirrors [6][14][23][28-29].
Focusing on aforementioned design constraints, various scanners are designed and proposed in this work. The most significant design parameters can be listed as follows: micro- scanner size, scan angle and structural material [12].

First of all, circular mirror shape is chosen for scanner design due to bending properties of thin plates as mentioned in [28]. Maximum deflection property of circular geometry makes this geometrical shape more favourable. Hence, as a future work, by use of an additional scanning mode, out of plane pumping, focus control can be improved with designed micro-scanner.

Therefore, in order to ensure high resonance frequency, scanner flexure lengths are kept as small as possible. Flexures and supports are designed in order to respect degrees of freedom mentioned above.

Furthermore, table top optical set-up limits scanner design. It is required to respect used instruments dimensions. Moreover, as it can be observed in Fig.4.1 and Fig.4.2, holes are anticipated on technical drawing in order to satisfy optical instruments dimensions.

In conclusion, various scanners are proposed enrich acknowledgement about behaviour and properties of scanners [4][14][16][18][20][22-24][29]. Proposed scanners are simulated.

Some design constraints are imposed in order to improve scanning features. For the proposed stainless steel scanner, magnetic actuation is preferred and the design is made accordingly. Proposed design is required to have a TOSA greater than 20°. It is aimed to have a high ratio between fast scan and slow scan frequencies. It is desired to realize two dimensional scanning by this proposed scanner.

.

The dimensions of the scanner providing a raster scanning are given in Table 2.2. L_s is length of scanner, Ws is width of scanner, L_{fo} is length of outer flexure, W_{fo} is width of outer flexure, t is thickness, D is diameter of mirror, L is length between two flexures, W is width of flexure and L_g is length of flexure gap.

Fig.2.1 demonstrates proposed scanner along with its design parameters.

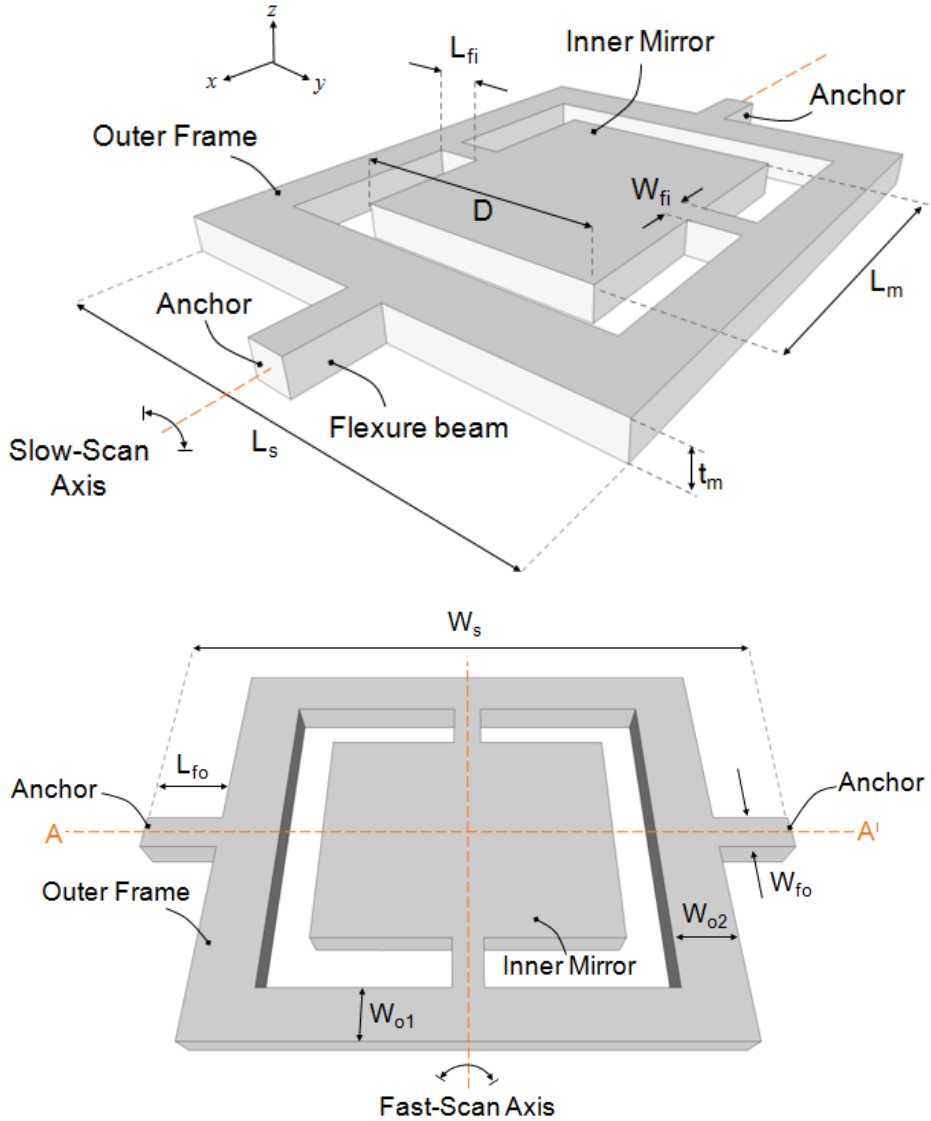

Figure 2.1. Dimensional (3D) drawing of the proposed scanner along with its parameters

Table 2.2. Dimensions of the proposed scanner

Parameter	Dimension (μm)	Parameter	Dimension (μm)
D	3600	W_{o1}	1830
L_m	9160	W_{o2}	3230
L_{fi}	1080	t_m	570
L_{fo}	1080	W_s	16160
W_{fi}	400	L_s	15490
W_{fo}	400		

The dimensions of the proposed scanner providing a raster scanning are given in Table 2.2. L_s is length of scanner, W_s is width of scanner, L_{fi} and L_{fo} are respectively lengths of inner and outer flexures, W_{fi} and W_{fo} are respectively widths of inner and outer flexures, t_m is thickness of scanner, D is scanner width, L_m is scanner length, W_{o1} and W_{o2} are respectively widths of proposed scanner.

3. SIMULATIONS

As in Fig.3.1, technical drawing of scanner design is completed in AutoCAD in appropriate format for simulations. Then, it is exported to simulation software, Comsol Multiphysics.

Finite element modelling (FEM) of scanner is performed with Comsol Multiphysics to determine fast and slow resonance frequency values and the related displacement values of proposed scanner. Resonance frequency values and displacement values are respectively shared in Table 3.1 and Table 3.2 for proposed scanner.

First 6 modes of proposed scanner are demonstrated in Fig.3.2. These modes correspond to different resonance frequencies of scanner. Behaviours of scanner are different for each frequency value.

As demonstrated in Fig.3.2, slow scan mode is come up as the first mode. It is important to achieve a high ratio of scan frequencies.
For proposed scanner, slow scan and fast scan frequencies are encountered in first 6 modes. Fig.3.2 (a) and Fig.3.2 (f) depict respectively slow scan frequency and fast scan frequencies.

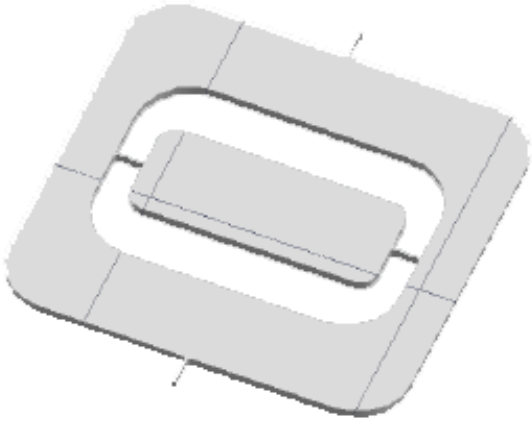

Figure 3.1. Technical drawing of proposed scanner for simulations

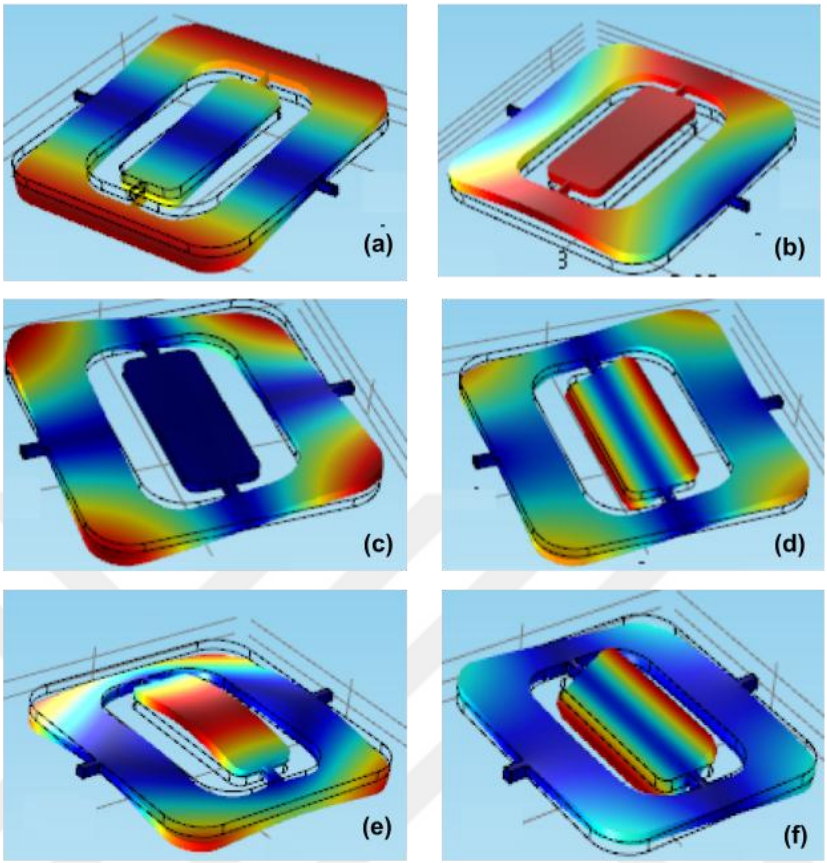

Figure 3.2. First six modes of the proposed scanner

Table 3.1. Resonance frequency of fast scan and slow scan

Resonance Frequency (Hz)	
Fast Scan	**Slow Scan**
120.73	12.56

Table 3.2. Displacements of fast scan and slow scan

Displacements (μm)	
Fast Scan	**Slow Scan**
8.19	3.21

Table 3.3. Resonance frequency values of first six modes of proposed scanner

Scan mode	**Scan mode resonance frequency (Hz)**
(a)	12.56
(b)	34.45
(c)	70.25
(d)	95.75
(e)	105.54
(f)	120.73

Resonance frequency values of proposed scanner depicted in Fig.3.2. are given in Table 3.3. The targeted modes (a) and (f) of the proposed scanner correspond to torsional modes, rotation around x-axis. They serve to realize two dimensional scanning. Then, Fig.3.2 (b) and (e) are pumping modes. Pumping mode is motion of a translation around z-axis. Moreover, Fig.3.2 (c) and (d) are in-plane rocking. This motion is rotation around z-axis.

As referred in Section 2, to enable increase resolution two torsional modes scanning frequencies must be far enough. This high-quality factor delivers large displacement of scanner. It is also important to notice that, when torsional mode comes up as first mode, this fact raises resonant frequency ratio. According to simulated results, slow resonance frequency is the first mode. Furthermore, slow and high resonance frequency values are adequately separated.

For the proposed scanner fast scan and slow scan frequencies ratio is 9.61. This ratio is considerably high for a good scanning.

As mentioned previously, high ratio between fast scan and slow scan frequencies increases resolution of images.

4. FABRICATION

In this section, fabrication of the proposed scanner is explained.

Proposed scanners are fabricated by laser-cutting process in cleanroom environment. For this process, PALS laser cutter machine is used. It is a fiber laser device operating by four axes.

The drawing prepared for cutting process is represented in Fig.3.1. Required drawing for this process in prepared in AutoCAD and exported to appropriate format.

Technical properties of this laser cutter are given in Table 4.1.

Table 4.1. Technical properties of laser cutter

Technical Properties of Laser Cutter Device	
Average output power	200 Watt
Operation modes	Continuous and unmodulated wave
Wavelength	1080 nm
Polarization	No
Modulation capacity	Unlimited shaping and operation loops
The smallest laser beam diameter	16 micrometer

The proposed stainless steel grade 430 scanner is fabricated by laser cutting process and Fig.4.1 demonstrates fabricated scanner.

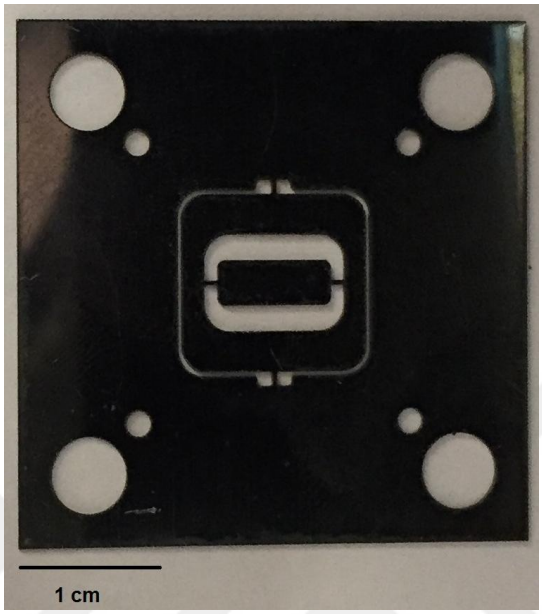

Figure 4.1. Fabricated SS grade 430 scanner

Fig.4.2 depicts fabricated scanner within the set-up.

Proposed scanner possesses some holes on scanner design are envisioned. These holes serve to assemble scanner to optical set up. In Fig.4.2, scanner is integrated to optical system.

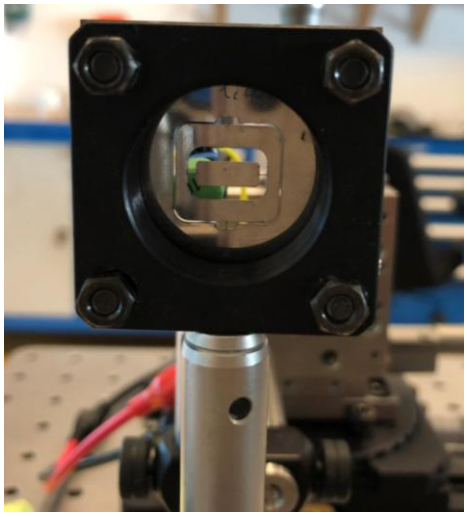

Figure 4.2. Fabricated SS grade 430 scanner within the set up

As a member of stainless steel (SS) family, SS 430 belongs to ferritic group of steels [30]. Material composition of SS is listed in Table 4.2 according to Hamilton SS430 datasheet. SS 430 composes of < 0.12% of carbon, C, approximately 16-18% of chrome, Cr, < 0.75% of nickel, Ni, < 1.0% of manganese, Mn, < 1.0% of silicon, Si, < 0.040% of phosphorus, P and < 0.03% of sulfur, S. Left part consists ferritic part. It is composed of iron, Fe.

Thanks to the magnetic properties of the stainless steel 430, it is preferred in several applications. Stainless steel makes part of soft magnetic materials. In other words, the material doesn't possess permanent magnetic property and to be able to gain its magnetic property, presence of a magnetic field is required. Since scanner is magnetically actuated, stainless steel represents favourable material properties. As it will be mentioned in Section 5, stainless steel represents good material properties for magnetic actuation. Magnetic actuation and magnetic behaviour of stainless steel material are elaborated in Section 5.

Table 4.2. SS Grade 430 composition

Stainless Steel Grade 430 Composition								
Metal	**Fe**	**C**	**Cr**	**Ni**	**Mn**	**Si**	**P**	**S**
Composition (%)		<0.12	16-18	<0.75	<1.0	<1.0	<0.040	<0.030

Stainless steel material can be readily cut. While cutting process, low heat is generated. It means that material properties aren't significantly affected [20] [31]. These reasons allow fabricating scanners by laser cutting technology. Though, for some scanner designs extremely small details are damaged while cutting process.

5. MAGNETIC ACTUATION

As it is mentioned in Section 1, MEMS structures can be predominantly actuated magnetically, electro statically, thermally or by piezoelectric methods.

Electrostatic actuation is largely served for actuation of silicon [32] and metal-based [33] structures. Whereas for electromagnetic actuation soft magnetic materials or hard magnetic materials can be used such as stainless steel, iron or cobalt alloys [2][34-35].

As previously mentioned, there are two principle magnetic actuation schemes namely, moving magnet and moving coil schemes. External magnets can also be used in order to generate static magnetic fields. Magnetic actuation enables achieving high optical scan angles with under low current application [24].

In order to utilize magnetic field in an optimum way, position of electro-coil and magnetic material properties are taken in account. Meanwhile, for a magnetically actuated system by an electro-coil, coils angular position according to micro-system is significant in order to make use of maximum magnetic field. An inclination allows the maximization of fast and slow scan images lengths.

$$TOSA\ (\theta) = 2\arctan(\frac{L/2}{X}) \tag{5.1}$$

where as in Fig.7.1, L is the image length, θ is TOSA and X corresponds to distance between scanner and image. According to Eq.5.1, increasing image length, L, increases also total optical scan angle. For this reason, coils are situated with an inclination as 45° [4][23-24].

Most part of magnetic actuation is provided only by a single electro-coil. To generate a static field, if it is required, an external magnet can be used. Solely, for magnetic actuation, it is also possible to place more than a single coil and make a coil array [36].

5.1. B-H Curve

Magnetic actuation is produced by the interaction between a magnetic material and an external magnetic field. Otherwise, some kind of magnetic materials such as ferromagnetic materials don't possess intrinsic magnetic properties in the absence of an external field.

As it can be observed from the B-H hysteresis curve in Fig 5.1, soft magnetic materials have low remanence (fraction of the saturation after magnetic field intensity ($\vec{H}$) is removed) and exhibit internal magnetization only while the presence of external magnetic field. Additionally, soft magnetic materials possess a narrow hysteresis loop. A narrow area defined by the curve signifies small quantity of stored energy. Due to this small quantity of energy, several advantages of soft magnetic family materials are come up, such as high efficiency, low power consumption and rapid transition.

Proposed electro-coil serves to create a magnetizing field $\vec{H}$ to actuate stainless steel (soft magnetic) scanners. A magnetic induction $\vec{B}$ is formed inside the material with the application of magnetic field, $\vec{H}$. Internal magnetization of material, $\vec{M}$, defines magnetization direction of material in the absence of an external magnetic field. In the absence of external magnetic field, magnetization vectors aren't aligned following a definite direction. [18-19]

The relation between magnetic field and magnetic induction can be expressed by following equation [18].

$$\vec{B} = \mu_0\vec{H} + \vec{M} = \mu_0 (\vec{H} + \chi \vec{H}) = \mu_r\mu_0\vec{H} \qquad 5.2$$

where μ_0 is the magnetic permeability of space, μ_r is the relative permeability of the magnetic material and χ is the susceptibility.

Generally, ferromagnetic materials are preferred for MEMS actuation applications. They have a large relative permeability. In other words, according to Eq.5.2 when relative permeability is increased magnetic field density is also increased.

Stainless steel scanners make part of ferromagnetic materials. Before application of an external magnetic field, global magnetization $\vec{M}$ of all the individual domains is zero. When a magnetic field is applied, domains are aligned in the same magnetic field direction.

$\vec{B}$ and $\vec{H}$ possess a non linear relationship. Though, in a certain interval of $\vec{H}$ values, $\vec{B}$ and $\vec{H}$ have a linear relationship and this can be illustrated by a hysteresis curve as in Fig.5.1. Hysteresis curve of magnetization explains linear behaviour of magnetic field and magnetic induction.

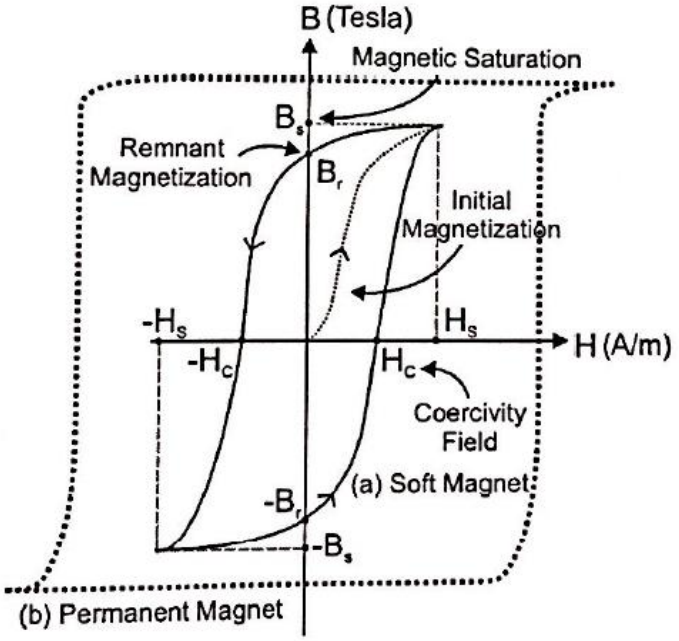

Figure 5.1. Hysteresis curve of soft magnet (a) and permanent magnet (b) [18]

Magnetic saturation point represents alignment of all available domains in a magnetic material. This alignment is observed in the case magnetic induction field has attained to its maximum value, on magnetic saturation point. Moreover, when magnetization is removed from the medium, a portion of magnetization is retained by material. This fact is called remanent magnetization. In other words, remnant magnetization indicates magnetization of material in absence of $\vec{H}$. Coercivity is required reverse field measure to bring magnetization to zero.

Closed path around the hysteresis curve shows magnetic energy amount in magnetic material. According to hysteresis curve, soft magnetic materials possess narrow hysteresis loop and coercivity is also small. The narrow hysteresis curve implies high efficiency, low power consumption and rapid transition [37]. Thus, this is what we need for stainless steel.

B-H curve of stainless steel grade 430 is demonstrated in Fig.5.2 [38]. As it is mentioned, due this narrow hysteresis curve, stainless steel is achieved high efficiency and rapid transition with low power consumption.

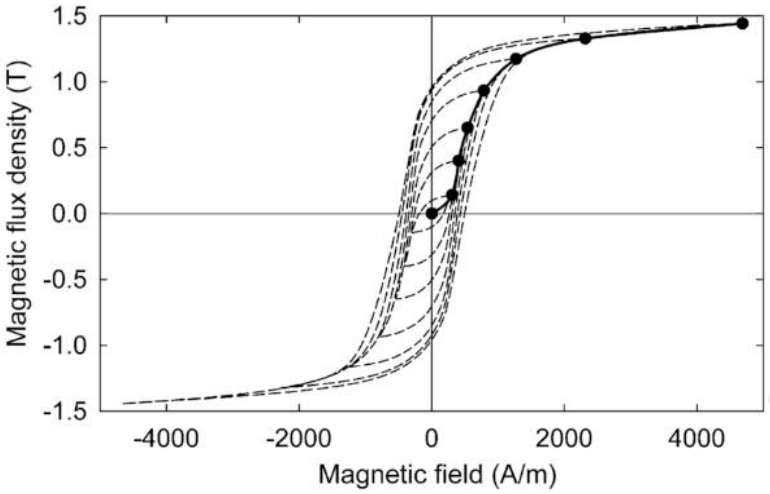

Figure 5.2. B-H curve of stainless steel grade 430

5.2. Equivalent Magnetic Circuit

Moving magnet actuation scheme used in this study is shown in Fig.5.2. In this system, aforementioned electro-coil provides NI ampere-turn magnetomotive force (MMF). The $\vec{H}$-field created by the electro-coil interacts with the soft- magnetic stainless steel.

When a negligible fringing field is assumed in the actuation system, the driving current I(w) shown in Fig.5.2 creates a $\vec{H}$-field inside the electro-coil and that is equal to Eq.5.3.

$$\vec{\mathrm{H}} = \frac{\mathrm{NI}}{\mathrm{L}} \tag{5.3}$$

where N is number of turns, I is driving current and L is length of electro-coil.

This actuation system depicted in Fig.5.2 can be modelled as a magnetic circuit. $\vec{H}$-field follows a closed path around the system. It stems from the electro-coil, passes through the air-gap (d_z) reaches to steel scanner with the dimensions of A µm to B µm and it is closed from the far-side of the electro- coil.

Stainless steel is a soft magnetic material for which an external magnetic field is required for magnetic actuation.

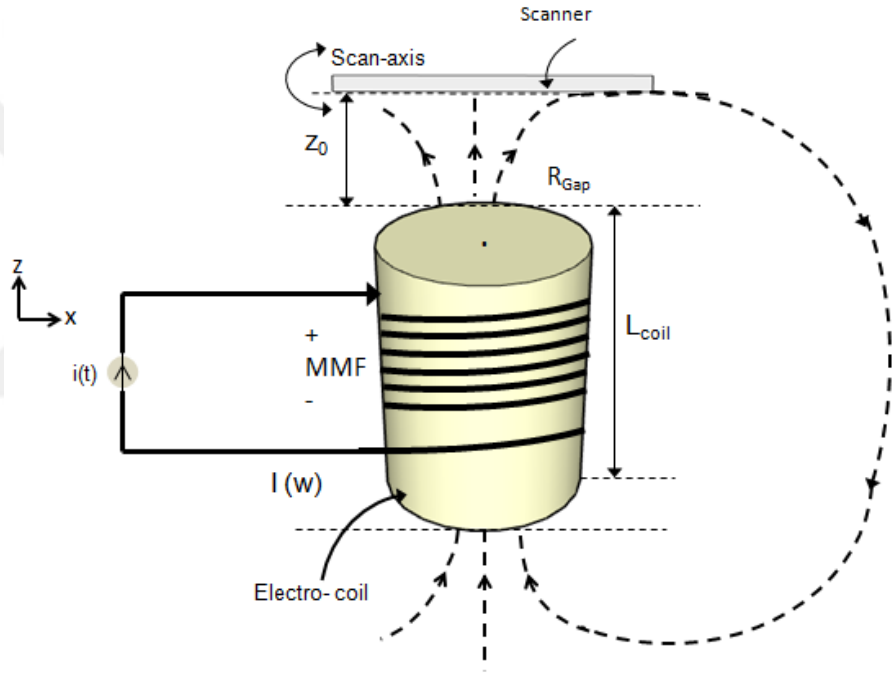

Figure 5.3. Magnetic actuation of micro- scanner by electro- coil

As illustrated in Fig.5.2, B-H curve, stainless steel has low remnant magnetization. Soft magnetic material cannot be magnetically actuated in the absence of an applied external magnetic field, because it isn't magnetized. In other words, magnetization vector is parallel to local external magnetic field (Liu, 2012). In application of an external magnetic field, stainless steel mechanical behaviour can be observed as mechanical forces and torque.
For actuation of stainless steel, a kind of soft magnetic material, either a magnetic gradient to attract or elongated shapes of soft material to rotate in uniform field are required.

Shape anisotropy is the fact that magnetization has tendency to lie along a specific axis (Gokdel Y. G., 2011) (Liu, 2012). If micro structure doesn't have a spherical form, more precisely if it has a linear form, the magnetization vector is in the scanning axis. The direction and intensity of this magnetization vector depends on external magnetic field.

Force exerted due this phenomenon, can be calculated by using Eq.5.4 (Gokdel Y. G., 2011).

$$F = \vec{M} W_s t \vec{H} \cos\theta \qquad 5.4$$

where W_s, t are the width and thickness of scanner, respectively. $\vec{M}$ represents magnetization vector and $\vec{H}$ is the magnetic field. $\vec{M}$ is related to the external field and the permeability. θ is the angle between scan axis and scanner.

It is important to remark that, while torsional motion of scanner the effect of net force can be neglected for the reason that exerted forces are in the opposite directions. Nevertheless, in the presence of an external magnetic field, torque acting on micro- structure has tendency to align magnetization vector and external magnetic field lines. Occurred torque value can be expressed and calculated as [18].

$$T = \vec{M}\vec{H}[W_s t L_{coil}] \cos\theta \qquad 5.5$$

6. ELECTRO - COIL DESIGN

As mentioned in previous chapters, moving magnet and moving coil schemes fulfil two fundamental magnetic actuations schemes required for magnetic actuation.

This section talks about design of an electro-coil in order to provide a magnetic actuation for scanner.

A permanent magnet can be a simple solution for magnetic interaction (fixed force or torque). Nevertheless, a permanent magnet generates a constant magnetic field which cannot be adjusted to desired magnetic field intensity. That's why, this magnetic field isn't suitable to be performed at desired frequency values. To create a variable, controlled magnetic field, the universal solution is a controlled, variable current inside an electro-coil.

With this perspective, an electro-coil is designed in order to provide a magnetic field at the determined frequency values. Fig.6.1 illustrates electro-coil parameters and position.

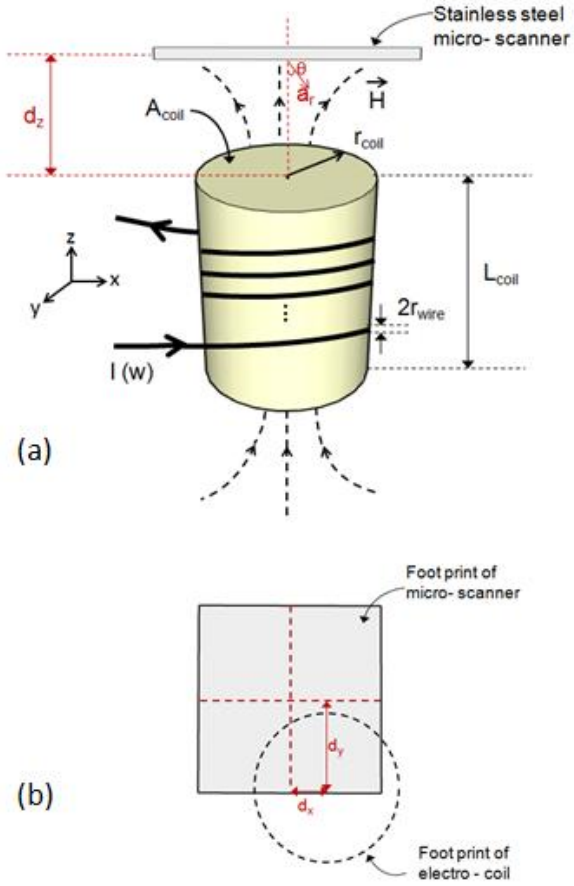

Figure 6.1. Illustration of electro-coil. a) side view b) top view

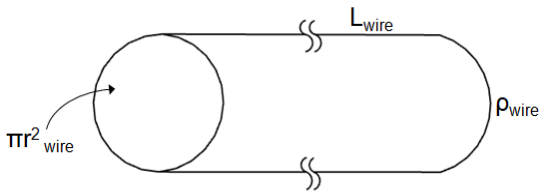

Figure 6.2. Illustration of coil wire

If we assume a wire with an insulating coating that has a cross-sectional area of A_{wire} and a length of L_{wire} and a radius of r_{wire} as depicted in Fig.6.2.

And if we assume a limited wire length and no overlapping turns, number of turns N can be computed as:

$$N = \frac{L_{coil}}{2r_{wire}} \tag{6.1}$$

Suppose that we provide a constant voltage drive to the electro-coil, the drive current becomes

$$I = \frac{V_{drive}}{Z_{coil}} \tag{6.2}$$

where

$$Z_{coil} = R_{coil} + X_L \tag{6.3}$$

where Z_{coil} is impedance of coil, R_{coil} is resistance of coil and X_L is inductance of coil.

Since the resonance frequency of the targeted modes of the proposed scanner is below 1 kHz, we can neglect X_L. In the other words Z_{coil} can be considered equal to R_{coil}.

$$R_{coil} = \rho_{wire} \frac{L_{wire}}{A_{wire}} \tag{6.4}$$

where

$$A_{wire} = \pi(r_{wire})^2 \tag{6.5}$$

and

$$L_{wire} = N2\,\pi r_{coil} \tag{6.6}$$

By using Eq.6.1,

$$L_{wire} = \frac{L_{coil}\, r_{coil}\pi}{r_{wire}} \tag{6.7}$$

Therefore, by plugging Eq.6.7 in Eq.6.4, R_{coil} becomes,

$$R_{coil} = \frac{\rho_{wire} L_{coil} r_{coil}}{r_{wire}^3} \quad 6.8$$

Thus, according to Eq.6.2 by plugging R_{coil},

$$I = \frac{V r_{wire}^3}{\rho_{wire} L_{coil} r_{coil}} \quad 6.9$$

According to Ampère's law, Eq.6.10 defines magnetic flux density,$\vec{B}$, in a closed loop path.

$$\oint_0^L \vec{B}\, dl = I\, \mu_0 \quad 6.10$$

Since a coil contains many linear paths, current value must be multiplied by N, number of turns.

Therefore,

$$\vec{B}L = IN\mu_o \quad 6.11$$

$$\vec{B} = \mu_o \frac{NI}{L} \quad 6.12$$

where

$$\vec{H} = \frac{\vec{B}}{\mu_o} \quad 6.13$$

L value, expressed in Eq.5.3, corresponds to coil length.

$$\vec{B} = \mu \frac{NI}{L_{coil}} \quad 6.14$$

where

$$\mu = \mu_o \mu_r \quad 6.15$$

If we consider the Eq.6.14, by plugging N and I, $\vec{B}$ formula is expressed as in Eq.6.16.

$$\vec{B} = \frac{\mu V r_{wire}^2}{2\rho_{wire} r_{coil} L_{coil}} \quad 6.16$$

Eq.6.16 proves that magnetic field significantly depends on coil parameters that are summarized on Table 6.1.

The magnetic flux created by the electro-coil is strongly related to radius of the wire cross section, r^2_{wire}, to the applied voltage V and relative permeability of the magnetic material and magnetic permeability of space whereas it is inversely proportional to resistivity of electro-coil material, radius and length of electro-coil.

Knowing that, magnetic permeability of space and permeability of the magnetic material are constants and a constant voltage drive applied to the electro-coil, parameters which are inversely proportional to magnetic field will mostly play role on electro-coil design.

Table 6.1. Electro-coil design parameters

	Design Parameters of Electro-Coil	**Designed Values**
N	Number of windings	500–700
L_{coil}	Length of coil (height)	12–14 mm
A_{coil}	Area of coil	
r_{coil}	Radius of coil	4 mm
ρ_{coil}	Resistivity of coil material	
A_{wire}	Area of wire	
r_{wire}	Radius of wire	
L_{wire}	Length of wire	
d_z	Distance between micro mirror and coil	
θ	Angle between micro mirror and coil	90°

Table 6.2. Electro-coil design constraints

Electro-Coil Design Constraints
Electro-coil volume is limited.
Large number of N is required to obtain maximum magnetic field.
Large value of I is necessary to provide maximum magnetic field.
Increasing length of coil also increases coil resistance.
To increase number of windings, A_{wire} must be small enough.
Small length of coil, L_{coil}, restrains maximizing the turn number N.
Optimum distances, Δd_x, Δd_y, Δd_z must be adjusted.
Optimum angle α must be adjusted.

Electro-coil design brings some constraints on geometry.

With respect to Eq.6.16, electro-coil volume is limited. For a planer coil, small value of L_{coil} is required. In order to obtain maximum magnetic field, number of windings, N, must be high enough. High value of L_{coil} enables high number of turns N. So, high magnetic field is generated. However, increased number of turns, N, augments L_{coil}. To respect volume constraints, A_{coil} and L_{coil} must be optimized. A_{wire} plays a role on number of windings.

Since wire section, A_{wire}, radius of coil, r_{coil} and length of coil, Lcoil, are limited, number of windings must be optimized according to these parameters. For instance, small length of coil, L_{coil} restrains maximizing number of windings. Increased r_{wire} decreases number of turns of wire because length of coil is determined. On the other hand, as mentioned in Eq.6.16, when radius of wire, r_{wire}, increases, magnetic field intensity increases proportionally.

Optimum distances, Δd_x, Δd_y, and Δd_z and optimum angle θ must be adjusted.

Since the proposed scanner has a dimension of approximately 16 mm x 16 mm, r_{coil} is limited to 5 mm in order to have a compatible size.

As shown in Eq.6.16 and assuming that coil wire is made of copper, coil design parameters depend significantly on coil parameters such as radius of coil, r_{coil}, and length of coil, L_{coil}. Magnetic field created by coil is inversely proportional to these parameters. Length of coil must be in accordance with scanner dimensions. Therefore, length of coil is limited to 15 mm.

Moreover, magnetic field increases with increasing radius of wire, r_{wire}. Nevertheless, radius of wire, r_{wire} must be also limited because it affects coil length with Eq.6.1. As mentioned previously, number of turns, N, increases substantially generated magnetic field as in Eq.6.14. Thereby, in order to rise number of turns, radius of wire must be chosen quite small and control magnetic field by inversely proportional parameters.

To enhance number of turns, radius of wire is chosen sufficiently smaller like 0.1 mm and by varying coil turns simulations are performed by Comsol Multiphysics 4.4.

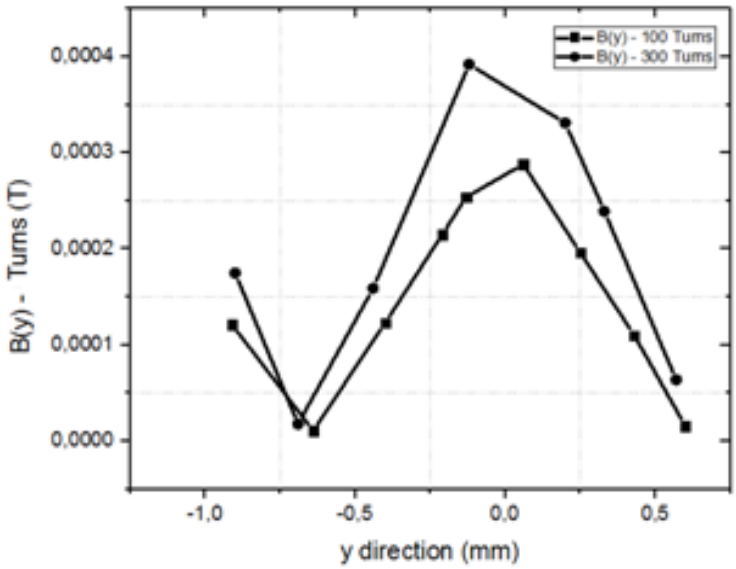

Figure 6.3. Magnetic field in y direction by varying number of turns

As it can be observed in graphic given in Fig.6.3, essentially, magnetic field intensity increases by increasing number of turns. Also, assuming directions on Fig.6.1, when we are moving away from electro-coil, magnetic field intensity drops.

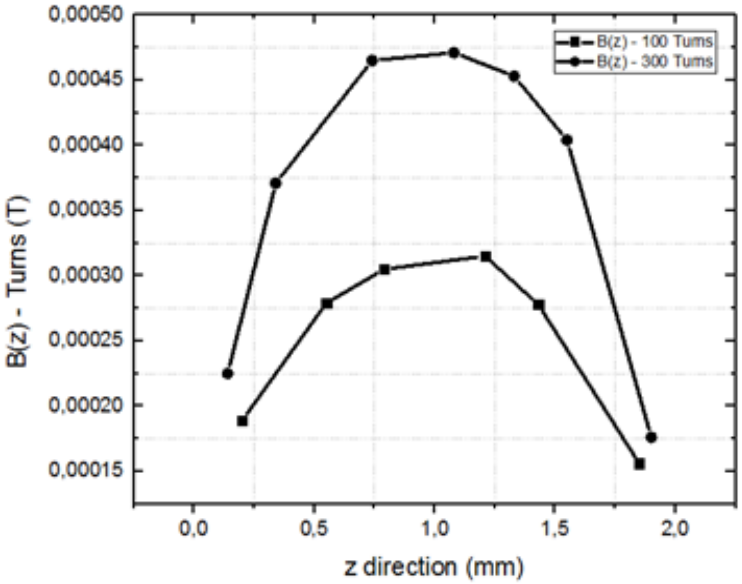

Figure 6.4. Magnetic field in z direction by varying number of turns

As in plot reported in Fig.6.4, magnetic field intensity decreases while moving to extremities of electro-coil even though number of turns increase. At the edge, magnetic field is the half of the centre.

Focusing on Fig.6.3 and Fig.6.4 and Eq.6.1, L_{coil} can be calculated and optimized.
Regarding Eq.6.8, resistance of coil, R_{coil} depends on ρ_{wire}, r_{wire}, L_{coil} and r_{coil}. Since resistivity and radius of wire and radius of coil are constants and predetermined variables, length of coil will determine significantly resistance of coil, R_{coil}. Increasing length of coil provokes a proportional raise of coil resistance. Hence, while choosing length of coil, this parameter must be taken in account. Obviously, increased resistance value isn't desired.

According to Eq.6.1, L_{coil} is calculated for a given number of turns N. L_{coil} is reported in Table 6.3 for a predetermined r_{wire} value.

As it can be observed in Table 6.3, when number of turns augments coil length gets longer. Relatively high numbers of turns must be preferred in order to increase magnetic field intensity. It is effectively required to contrive conformity between numbers of turns in order to increase magnetic field intensity and length of coil to respect scanner dimensions.

Table 6.3. Optimization of electro-coil length

Electro-coil Length Optimization		
r_{wire} (mm)	**N**	**L_{coil} (mm)**
0.01	100	2
0.01	300	6
0.01	400	8
0.01	500	10
0.01	600	12
0.01	650	13
0.01	700	14
0.01	750	15

By using Eq.6.8, in the same manner, resistance of coil can be calculated in function of varying coil length. Material of the electro-coil wire is chosen as copper because of its better conduction properties compared to other metals such as aluminium. The wire resistivity, ρ_{wire}, is $1.72.10^{-8}$ Ωm. Radius of wire is 0.01 mm. The radius of coil is restricted to 5 mm to have appropriate dimensions with micro-scanner. The variation of electro-coil resistance in function of length of electro-coil is given in Table 6.4.

Table 6.4. Resistance of coil

Resistance of Electro-coil in function of Coil Length			
r_{coil} = 4 mm		**r_{coil} = 5 mm**	
L_{coil} (mm)	**R_{coil} (Ω)**	**L_{coil} (mm)**	**R_{coil} (Ω)**
10	$6.88.10^{-8}$	10	$8.6.10^{-8}$
12	$8.256.10^{-8}$	12	$1.032.10^{-7}$
13	$8.944.10^{-8}$	13	$1.118.10^{-7}$
14	$9.632.10^{-8}$	14	$1.204.10^{-7}$
15	$1.032.10^{-7}$	15	$1.29.10^{-7}$

As mentioned beforehand, length of coil is limited to 15 mm in order to have compatible size. Therefore, number of turns can be between 500–750 which corresponds to 10-15 mm of length. Table 6.4 represents resistance of coil in function of varying coil length. Assuming la multiplication of radius of coil by length of coil as volume of coil, when dimensions of coil get higher resistance goes up. As a result, radius of coil can be chosen 4 mm, not 5 mm because for 5 mm of radius, R_{coil} increases more significantly than 4 mm radius. Furthermore, a measure between 12–14 mm of coil length selection is appropriate for scanner design. Briefly, Table 6.1 indicates designed values.

According to all optimization calculations, simulations and implications, required electro-coil length must be 12-14 mm with a radius of 4 mm to respect determined constraints.

Since electro-coil fabrication is considerably difficult, regarding design parameters and desired electro-coil dimensions, an off-the-shelf coil which is the most appropriate is utilized within de content of this thesis. Dimensions of this electro-coil are given in Table 6.5. Inductance of electro-coil is approximately 108 mH. Its radius is 4 mm and its length is 12.28 mm.

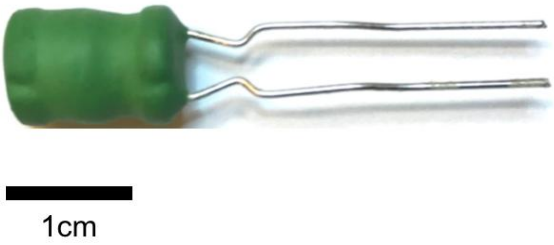

Figure 6.5. Off-the-shelf coil

Table 6.5. Dimensions of off-the-shelf coil

Electro-coil Dimensions (mm)		
r_{coil}	Radius of coil	4
D_{coil}	Diameter of coil	8.07
L_{coil}	Length of coil	12.28
r_{wire}	Radius of wire	0.01

7. ACTUATION OPTIMIZATION AND EXPERIMENTAL RESULTS

In this section, electro-coil position with respect to scanner is optimized in order to achieve a high total optical scan angle (TOSA).

With the purpose of increasing TOSA and improving scanning features, electro-coil and scanner positions and inclination of magnetically actuated systems are adjusted. The inclination allows maximizing TOSA by increasing image lengths.

Total optical scan angle can be achieved by Eq.5.1, as below:

$$TOSA\ (\theta) = 2\arctan(\frac{L/2}{X}) \qquad 5.1$$

where L is the image length, θ is TOSA and X is the distance between scanner and image.

Assume that angle θ is equal to 2 times α, as in Fig.7.1. Thus, angle value of Eq.5.1 must be multiplied by two. In Fig.7.1, image length corresponds to width and angle corresponds to scan angle. Distance is represented by x and it is between scanner and screen.

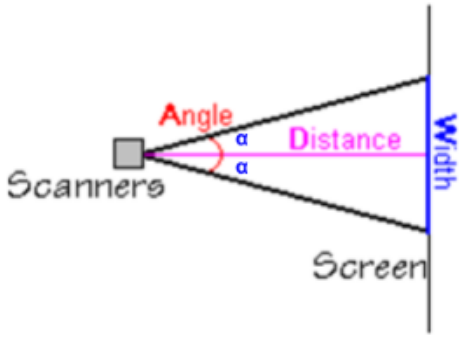

Figure 7.1. Analytical calculation of TOSA

As it is mentioned, electro-coil position according to micro-system is significant not only to make use of maximum magnetic field but also to trigger simultaneously fast scan and slow scan frequencies. In this perspective, for optimization of electro-coil and scanner positions, electro-coil is moved in x, y and z directions of Fig.6.1, respectively. 0 mm is assumed as centre of scanner. Then, image length on screen is monitored and measured experimentally. Finally, TOSA is analytically calculated by Eq.5.1.
Corresponding setup for mentioned measurement is demonstrated in Fig.7.2.

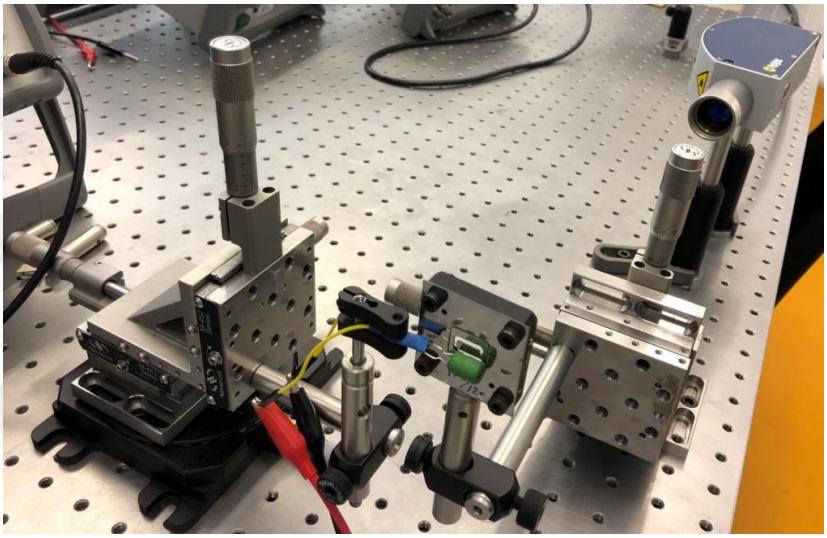

Figure 7.2. TOSA optimization set-up

The peak-to-peak voltage is 10 V. The distance between scanner and display is 152.4 cm. Fast scan and slow scan lines obtained by the set-up in Fig.7.2 are demonstrated in Fig.7.3 and Fig.7.4.

Figure 7.3. Slow (vertical) scan line

Figure 7.4. Fast (horizontal) scan line

With respect to constructed set-up in Fig.7.2, electro-coil position is varied in three directions and TOSA plots are reported.

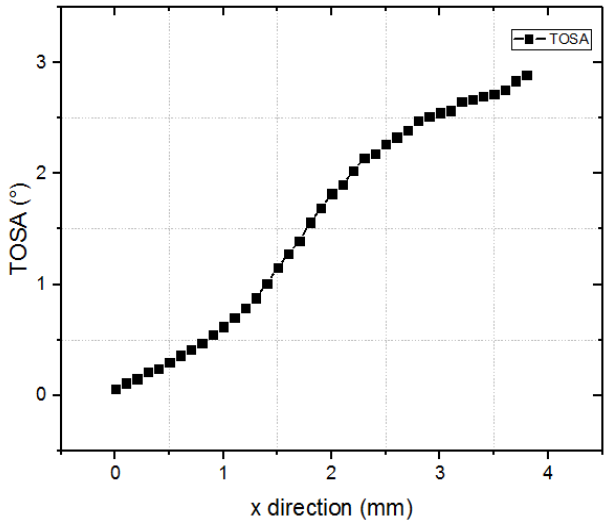

Figure 7.5. TOSA optimization in x direction

The x direction represents horizontal axis of electro-coil. Electro-coil is moved along this horizontal axis and image length is measured to calculate TOSA. Assume 0 mm corresponds to center of scanner and electro-coil is moved from center to extremities of horizontal axis. This axis is also slow scan axis of scanner. As observed in Fig.7.5, larger TOSA is achieved when electro-coil is moved away from center of scanner. Magnetic field force has higher torque and facilitates torsion motion. Thereby, since high TOSA is achieved from 3.5 mm, regarding Fig.7.5, it is more favourable to place electro-coil at 3.8 mm.

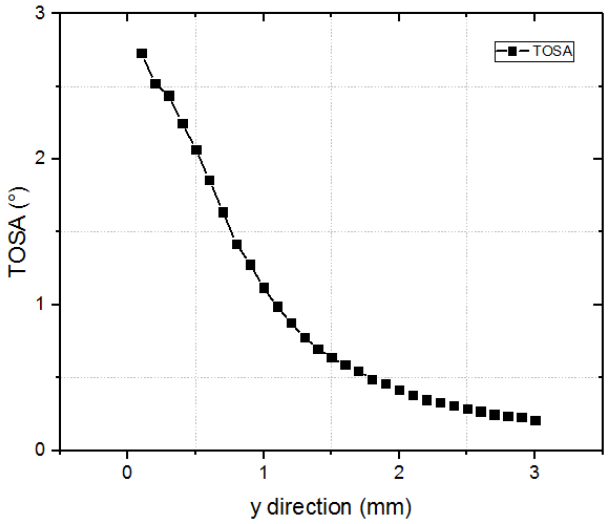

Figure 7.6. TOSA optimization in y direction

As observed from Fig.7.6, variation of TOSA in y direction, when coil distance between electro-coil and scanner increases, magnetic force acting on scanner decreases. Therefore, movement of scanner drops. In other words, when electro-coil moves away from scanner, magnetic field effect decreases. Thus, magnetic field intensity drop causes image length decrease and TOSA decrease as well.

Assuming 0 mm as a centre of scanner, electro-coil must be relatively close to scanner. Electro-coil must be placed approximately at 0.2 mm where TOSA is measured considerably high.

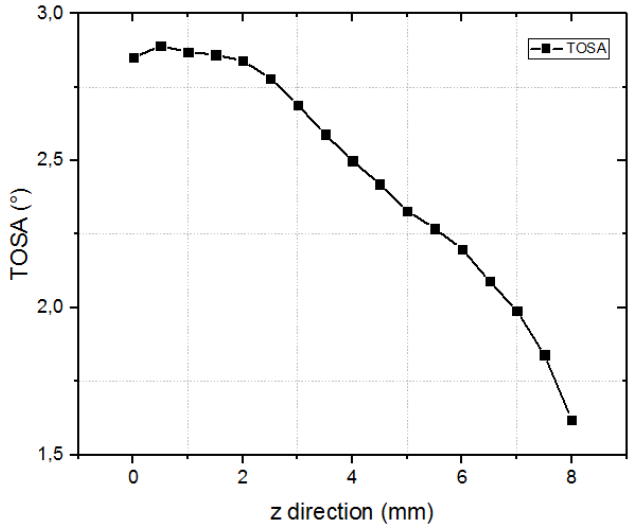

Figure 7.7. TOSA optimization in z direction

The z direction represents vertical axis of electro-coil. As plotted in Fig.7.7, starting from the center of coil, at 0 mm, while moving on extremities of scanner, since displacement of scanner decreases, image length decreases as well. It is especially better to place electro-coil close to the center of scanner, at 0.8-1 mm. This axis corresponds also to fast scan axis of scanner as it can be observed in Fig.4.2.

Angular optimization of electro-coil with respect to scanner is also optimized in order to increase TOSA. Distance between electro-coil and scanner is adjusted to 0.1 mm. Distance between scanner and display is 890 mm.

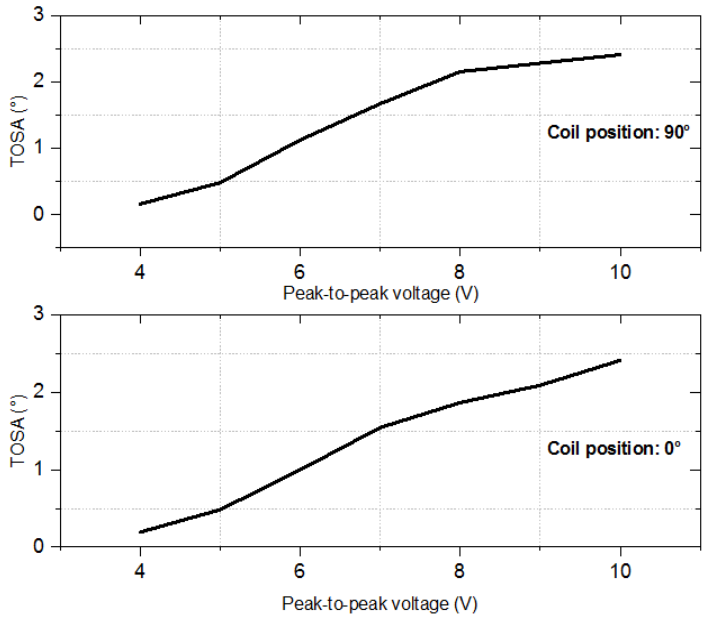

Figure 7.8. Electro-coil angular position

By varying electro-coil angle with respect to scanner and peak-to-peak voltage value, image length on screen is monitored and measured. In Fig.7.8, calculated TOSA angles are plotted for 0° and 90°. According to obtained results, as electro-coil position, 90° is appropriate because image lengths are longer. Thus, it allows increasing TOSA value.

Moreover, designed both scanners are characterized by Laser, Doppler Vibrometer, LDV device. LDV is a precision instrument which serves to detect vibrations without any contact. It is used for measuring displacement of scanners in different frequency values. Related measurement set up is given in Fig.7.9.

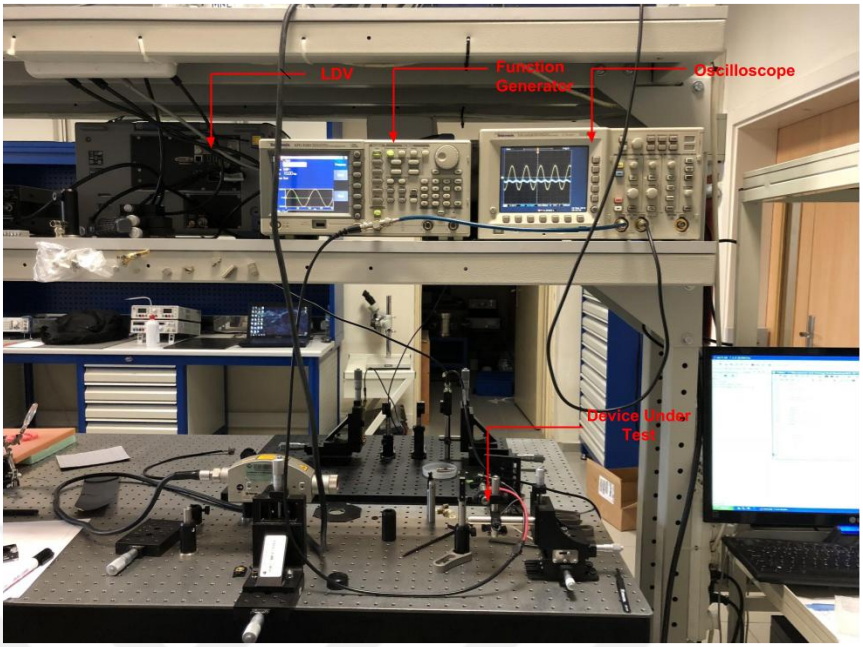

Figure 7.9. LDV characterization set up

LDV characterization of proposed scanner is plotted in Fig.7.10. The reported plot concerns displacement of scanner in function of frequency.

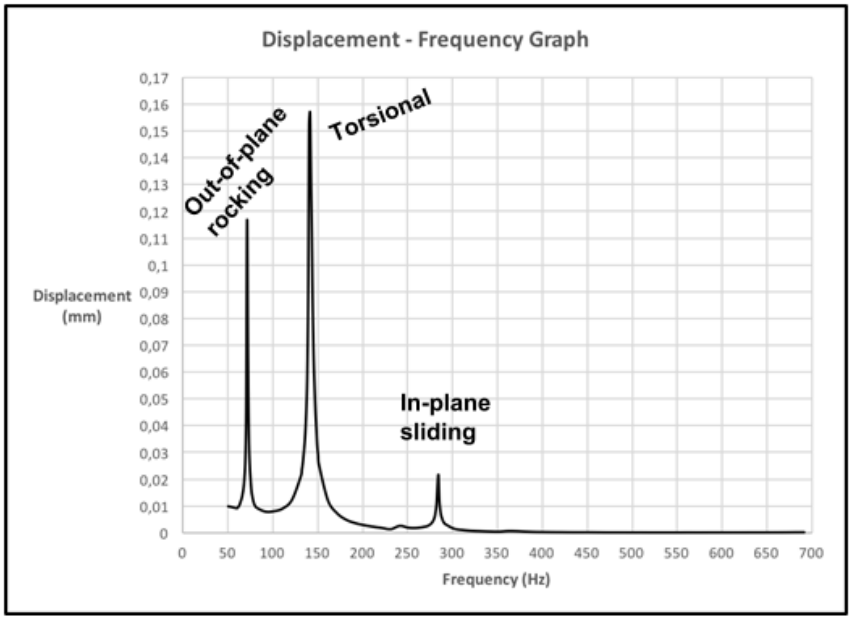

Figure 7.10. LDV characterization of proposed scanner

As in plot in Fig.7.10, proposed scanner has larger displacements approximately at 70 Hz, 140 Hz and 280 Hz. Once again LDV plots indicate displacement of proposed scanner in different modes at different frequencies.
Since proposed scanner has greater displacements at resonance frequencies, resolution of this scanner will be high.

Consequently, corresponding modes LDV and simulation frequency values are given in Table 7.1.

Table 7.1. LDV and simulation resonance frequency comparison

Vibration mode	**LDV frequency (Hz)**	**Simulation frequency (Hz)**	**Error (%)**
Out-of-plane rocking	70	70.2	0.2
Torsional	140	120.7	13.7
In-plane sliding	280	291.9	4.25

Table 7.1 compares resonance frequency values of different modes obtained by LDV characterization. As plot in Fig.7.10 reports maximum displacements are achieved in these frequency values. Corresponding modes are matched with modes in Fig.3.2. Then simulated frequency values are compared with LDV frequency values.

8. CONCLUSION

The research reported in this thesis consists of the optimization of magnetically actuated steel scanner systems. The distance between electro-coil and scanner according to x, y and z directions and rotation angle are optimized.

First of all, for this optimization, various two-dimensional scanners are designed. According to high and low scan frequencies, the best structure is chosen and is fabricated by laser cutting technique. Scanner has 5 mm of mirror diameter and 460 µm thickness.

Then, since scanner is magnetically actuated, electro-coil conceived to lead magnetic actuation as mentioned. In order to generate required magnetic field, electro-coil magnetic field formula is expressed versus coil parameters. In accordance with derived expressions, in the same way, an electro-coil is designed. Simulations results show that when number of turn increases, magnetic field intensity generated by coil goes up as well. Moreover, coil length must be compatible to scanner dimensions. Therefore, radius of coil is limited to 5 mm like length of coil. Derived equations indicate that length of coil determines resistance of coil. That's why resistance of coil is calculated respect to different length of coil dimensions. Achieved results of these calculations emphasize that increasing dimensions of coil makes increases coil resistance.

Consequently, according to achieved analytical calculations and simulation results, an electro-coil length of 12 mm with 600 turns for magnetic field generation. Due difficult fabrication process of coil, in spite of fabricate optimized electro-coil, similar off-the-shelf coil is used for experiments.

Continuing, in this context, in order to achieve the best total optical scan angle, distance between electro-coil and scanner is optimized in three dimensions with rotation angle.

Experimental results allow evaluating the most optimized position for electro-coil. It must be close enough to scanner because when electro-coil moves away from soft magnetic micro-structure, magnetic field intensity which serves to provide magnetic actuation

decreases. Efficiency of actuation is lost. Since magnetic field intensity decreases, image length decreases in a proportional way. Thus TOSA value drops.
Then, when electro-coil is placed through centre of scanner on scanning axes but through extremities delivers better images because increasing torque improves total optical scan angle.

In conclusion, optimized coil position is depicted in Fig.8.1. Angle α between scanner and electro-coil is considered as 90°. Optimized positions on x, y and z directions are 3.8 mm, 0.2 mm and 0.8 mm, respectively.

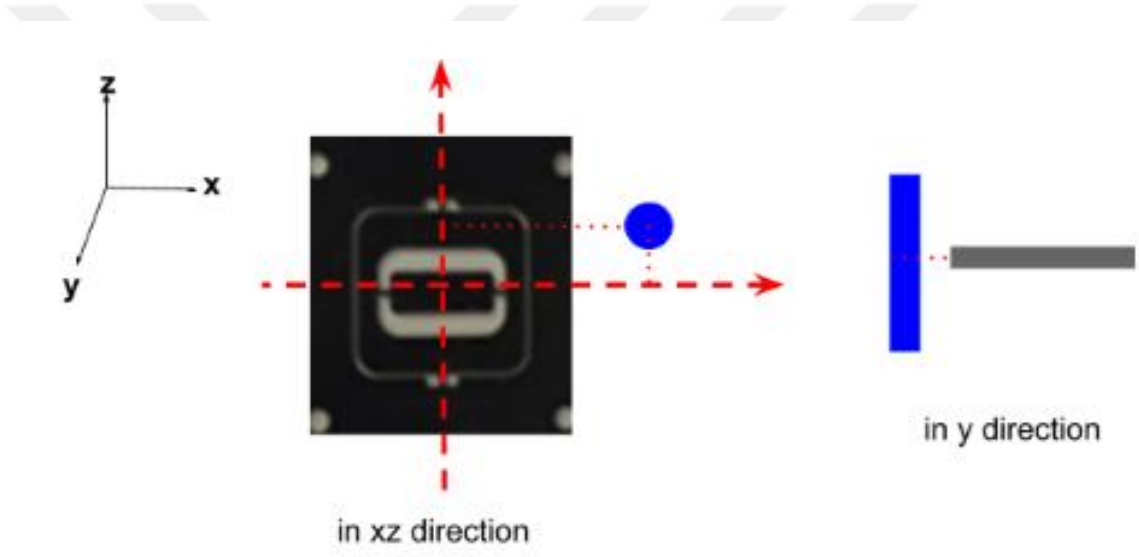

Figure 8.1. Electro-coil position optimization

This optimized position of the electro-coil can be expressed in a form of equation. The value of magnetic field intensity generated by the electro-coil can be calculated by Eq.8.1.

$$\vec{B}\,(x,y,z) = (3.8x\vec{x} - \ 0.2y\vec{y} + \ 0.8z\vec{z})sin\theta \qquad 8.1$$

9. REFERENCES

[1] Solgaard, O., Godil, A. A., Howe, R. T., Fellow, Lee and Pet, L. P., "Optical MEMS: From Micromirrors to Complex Systems", *Journal of Microelectromechanical Systems*, vol. 23, pp. 517- 538, 2014.

[2] Holmström, S. T. S., Baran, U., Urey, H., "MEMS Laser Scanners: A Review", Journal of Microelectromechanical System", vol. 23, pp. 259-275, 2014.

[3] Ataman, C., Lani, S., Noell, W., Rooji, N., "A Dual- axis Pointing Mirror with Moving- Magnet Actuation", *Journal of Microelectromechanical Systems*, vol. 23, pp. 025002, 2012.

[4] Yalcinkaya, A. D., Urey, H., Brown, D., Montague, T., Sprague, R., "Two- Axis Electromagnetic Microscanner for High Resolution Displays", *Journal of Microelectromechanical Systems*, vol. 15, pp. 786-794, 2006.

[5] Yalcinkaya, A. D., Urey, H., Holmstrom, S., "NiFe plated biaxial MEMS Scanner for 2- D imaging", *IEEE Photonics Technology Letters*, vol. 19, pp. 330-332, 2007.

[6] Hung, A. C.-L., La, H. Y.-H., Lin, T-W., Fu, S-G., Lu, M. S.-C., "An Electrostatically Driven 2D Micro- Scanning Mirror with Capacitive Sensing for Projection Display", *Sensor and Actuators A*, vol. 222, pp. 122-129, 2014.

[7] Toledo, J., Ruiz- Diez, V., Diaz, A., Ruiz, D., Donoso, A., Bellido, J.C., Wistrela, E., Kucera, M., Schmid, U., Hernando- Garcia, J., Sanchez- Rojas, J. L., "Design and Characterization of In- Plane Piezoelectric Microactuators", *Actuators*, vol. 6, pp. 1-13, 2017.

[8] Qui, J., Slocum, J. H., Strümpler, R., "A High Electrothermal Bistable MEMS Relay," in *In Proceeding of the IEEE Sixteenth Annual International Conference on Micro Electro Mechanical Systems*, Kyoto, Japan, 19-23 January 2003.

[9] Isikman, S. O., "Electromagnetically Actuated Optical Micro- Mechatronic Systems Integrated on PCB," Koç University, Istanbul, 2008.

[10] Tuantranont, A., Bright, V. M., "Introduction to Micro-Electro-Mechanical Systems (MEMS) with Emphasis on Optical Applications", *NEOTEC Technical Journal*, vol. 1, pp. 227-236, 2000.

[11] Urey, H., Wine, D. W., Osborn, T. D., "Optical Performance Requirements for MEMS- scanner Based Microdisplays", *Proc SPIE,* vol. 4178, pp. 1667-1675, 2000.

[12] Urey, H., Wine, D. W., Lewis, J. R., "Scanner Design and Resolution Tradeoffs for Miniature Scanning Displays", *Proc. SPIE,* vol. 3636, pp. 60-68, 1999.

[13] Gokdel, Y.D., Sarioglu, B., Mutlu, S., Yalcinkaya. A., "Design and Fabrication of Two- axis Micromachined Steel Scanner," *Journal of Micromechanics and Microengineering,* vol. 19, pp. 075001-1- 075001-8, 2009.

[14] Iseki, T., Okumura, M., Sugawar, T., Kurosawa, M. K. , "Deflection Properties of a MEMS Optical Scanner With Four Torsion Beams and L- Shaped Arms", *Sensors and Actuators,* vol. 178, pp. 154-163, 2011.

[15] Lee, S., Kim, M. G., Jun, M., Moon, S. H., Lee, J. H., "A MEMS Scanner with Four Orthogonally Arranged Rotators Actuated by Electromagnetic Force", in *Optical MEMS and Nanophotonics,* Cleanwater, FL, USA, 17-20 August 2009.

[16] Sunghoon, K., Milanovic, V., Lee, L. P., "A High Aspect Ratio 2D Gimbaled Microscanner with Large Static Rotation" *IEEE/ LEOS International Conference on Optical MEMS,* Lugano, Switzerland, Switzerland, pp. 149-150, 2002.

[17] Hofmann, U., Janes, J., Quenzer, H. J., "High- Q MEMS Resonators for Laser Beam Scanning Displays", *Micromachines,* vol. 3, pp. 509-528, 2012.

[18] Gokdel, Y. D., "Realization of Two- Dimensional MEMS Based Displays Using Polymer Composite Microscanners Integrated With One- Dimensional Polymer LED Arrays," Bogaziçi University, Istanbul, 2011.

[19] Miyajima, H., Asaoka, N., Isakawa, T., Aoki, Y., Imai, M., Fujimori, O., Katashiro, M., Matsumoto, K., "A MEMS Electromagnetic Optical Scanner for a Commercial Confocal Laser Scanning Microscope", *Journal of Microelectromechanical Systems,* vol. 12, pp. 243-251, 2002.

[20] Gokdel, Y. D., Mutlu, S., Yalcinkaya, A. D., "Self – Terminating Electrochemical Etching of Stainless Steel for The Fabrication of Micro–mirrors", *Journal of Micromechanics and Microengineering*, vol. 20, pp. 095009-095014, 2010.

[21] Urey, H., "Torsional MEMS Scanner Design for High- Resolution Display Systems", *Optical Scanning II, Proc. SPIE,* vol. 4773, pp. 27-37, 2002.

[22] Petersen, K. E., "Silicon Torsional Scanning Mirror," *IBM J. Res. Develop,* vol. 24,

pp. 631- 637, 1980.

[23] Ji, C. H., Choi, M., Kim, S. C., Song, K. C., Bu, J. U., Nam, H. J., "Electromagnetic Two-Dimensional Scanner Using Radial Magnetic Field", *Journal of Microelectromechanical Systems,* vol. 16, pp. 989-996, 2007.

[24] Oyman, H. A., Icel, M. A., Efe. B. C., Gokdel, Y. D., Ferhanoglu, O., Yalcinkaya, A. D., "A Laser- Machined Stainless Steel Micro- Scanner for Confocal Microscopy," in *Proceedings of Eurosensors 2017,* Paris, France, 3- 6 September 2017.

[25] Neukermans, A. P., Slater T. G., "Micromachined Torsional Scanner". U.S. Patent, t 5, 629 790, 1997.

[26] Urey, H., Kan, C., Davis, W., "Vibration Mode Frequency Formulae for Micromechanical Scanners", *Journal of Micromechanics and Microengineering,* vol. 15, pp. 1713-1721, 2005.

[27] Ran Hsu, T., "Engineering Mechanics for Microsystems Design", *MEMS and Microsystems- Engineering Science for Microsystems Design and Fabrication*, pp. 109-119, pp. 165- 177, McGraw-Hill, 2002.

[28] Ran Hsu, T., "Engineering Mechanics for Microsystems Design", in *MEMS and Microsystems - Engineering Science for Microsystems Design and Fabrication*, pp. 109- 119, 165- 177.

[29] Soemers, H., Krastev, K., Lierop, D. V., "Design of a High Frequency MEMS Scanning Mirror", *Allen Institute for Artificial Intelligence*, 2008.

[30] "Hamilton Precision Metals Sheet-SS430 Technical Data," 20 March 2001. [Online]. Available: https://www.hpmetals.com/-/media/ametekhpmetals/files/technical-data/stainless-steel/ss%20430.pdf.

[31] Coey, J. M. D., Magnetism and Magnetic Materials, Cambridge, 2009.

[32] Schenk, H., Durr, P., Haase, T., Kunze, D., Sobe, U., Lakner, H., Kuck, H., "Large Deflection Micromechanical Scanning Mirrors for Linear Scans and Pattern Generation", *IEEE Journal of SelectedTopics in Quantum Electronuic*, vol. 6, pp. 715-722, 2000.

[33] Buhler, J., Funk, J., Korvink, J. G., Steiner, F. P., "Electrostatic Aluminum Micromirrors Using Double Pass Metallization", *IEEE Journal of Microelectromechanical Systems,* vol. 6, pp. 126-135, 1997.

[34] Yalcinkaya, A. D., Ergeneman, O., Urey, H., "Polymer Magnetic Scanner for Bardcode Reader Applications", *Sensors and Actuators*, vol. 135, pp. 236-243, 2006.

[35] Isikman, S. O., Ergeneman, O., Yalcinkaya, A. D., Urey, H., "Modeling and Characterization of Soft Magnetic Film Actuated 2-D Scanners", *IEEE Journal of Selected Topics in Quantum Electronics*, vol. 12, pp. 283-289, 2007.

[36] Divoux, C., Cugat, O., Reyne, G., "Deformable Mirror using Magnetic Membranes: Application to Adaptive Optics in Astrophysics", *IEEE Transactions on Magnetics*, vol. 3, pp. 3564-3567, 1998.

[37] Liu, C., *Foundation of MEMS*, pp. 303-330, Pearson, 2012.

[38] Molt, R.W., Oxley, P., Goodell, J., "Magnetic Properties of Stainless Steels at room and Cryogenic Temperatures", *Journal of Magnetism and Magnetic Materials*, Vol. 321, pp. 2107-2114, 2009.

REFERENCES NOT CITED

Bourouina, T., Fujita H., Reyne, G., Motamedi, M., E., "Optical Scanning", *Micro- Opto-Electro- Mechanical Systems, SPIE,* pp. 323-367, 2005.

Urey, H., Holmstrom, S., Yalcinkaya, A. D., "Electromagnetically Actuated FR4 Scanners", *IEEE Photonics Technology Letters,* Vol. 20, pp. 30-32, 2008.

Weber, N., Zappe, H., Seifert, A., "An All- nickel Magnetostatic MEMS Scanner", *Journal of Micromechanics and Microengineering,* Vol. 22, pp. 125008-1-125008-7, 2012.

Shokouhian, S. B., Karimian, A., Mohammad- zadeh, M., Salighe-rad, H. R., "Designing and Fabrication of a New Radiofrequency Planar Microcoil for Mini- Nuclear Magnetic Resonance", *Iranian Journal of Medical Physics,* Vol. 13, pp. 193-202, 2016.

Hamilton, N., C., "Ferrites: magnetic and electric equivalent circuits and the complex permeability spectra", *IET Active and Passive RF Devices Seminar*, 2016.

Laith, E. R., "Magnetic Equivalent Circuits for Electrical Machines", *PROC. IEEE,* Vol. 114, No. 11, 1967.

Heteren J. G., Henkelman R. M., Bronskill M. J., "Equivalent Circuit for Coil – Patient Interactions in Magnetic Resonance Imaging", *Pergamon Journals,* Vol. 5, pp. 93-99, 1987

Tilmans, H. A., "Equivalent Circuit Representation of Electromechanical Transducers: I. Lumped- Parameter Systems", *Journal of Micromechanics and Microengineering*, Vol. 6, pp. 157- 176, 1996.

Senturia, S. D., Microsystem Design, Springer, 2000.

Palomar Technologies, “Micro-Optoelectronic Mechanical Systems (MOEMS)” [online], http://www.palomartechnologies.com/applications/micro-optoelectronic-mechanical-systems. [retrieved May 29, 2018]

Conant, R., “Micro machined Mirrors”, [online book], https://books.google.com.tr/books?id=l5zlBwAAQBAJ&pg=PA38&lpg=PA38&dq=total+optical+scan+angle&source=bl&ots=36hK7bwVeV&sig=ilHtfputhQ3W1abRf-Cwb5ojtvA&hl=fr&sa=X&ved=0ahUKEwigg8ykkv3JAhVGuhQKHSKICEYQ6AEILzAE#v=onepage&q=total%20optical%20scan%20angle&f=false [retrieved May 29, 2018]

Mohammed J. Moghimi, Krishna N. Chattergoon, Chris R. Wilson, and David L. Dickensheets, “High Speed Focus Control MEMS Mirror with Controlled Air Damping for Vital Microscopy”, *Journal of Microelectromechanical Systems*, Vol. 22, pp. 938-948, 2013.

Claire Max, “Deformable Mirrors, Lecture 8”, Astro 289, 4 February 2016.

Md. Mahabub Hossain, Wu Bin, Seong Ho Kong, “Electromagnetically Controlled Convex Micro mirror for Focal Length Variation”, 2015 *IEEE Sensors*, Bouson-South Korea, 2015.

Lukes, S. J., Dickensheets, D. L., “SU- 8 2002 Surface Micromachined Deformable Membrane Mirrors”, *Journal of Microelectromechanical Systems*, Vol. 22, pp. 94-106, 2013.

Sato, K., Okutsu, K., “Basic Characteristics of a Micromechanical Optical Switch Using an S-Shaped Deformable Thin – Film Mirror”, *Journal of Lightwave Technology*, Vol.29, pp. 2805-2811, 2011.

Cugat, O., Basrour. S., Divoux, C., Mounaix, P., Reyne, G., “Deformable Magnetic Mirror for Adaptative Optics : Technological Aspect”, *Sensors and Actuators*, Vol. 89, pp. 1-9, 2001.

Practical MEMS, Ville Kaajakari, Ch 18, Micro- Optical Devices.
Warren C.Young, Richard G. Budynas “Roark’s Formulas for Stress and Strain”, Seventh Edition, Chapter 11.

Arnold, P. A., Wang, N., “Permanent Magnets for MEMS”, Journal of Microelectromechanical Systems, Vol. 18, pp. 1255-1266, 2009.

Naono T., Fujii, T., Esashi, M., Tanaka, S., “A large-scan-angle piezoelectric MEMS optical scanner actuated by a Nb-doped PZT thin film”, Journal of Micromechanics and microengineering, Vol.24, Published 9 Dec. 2013, 2014.